DETECTING SPIDER MITE DAMAGE IN COTTON THROUGH SPECTRAL MIXTURE ANALYSIS OF AVIRIS IMAGERY

Glenn J. Fitzgerald[1]
Steve J. Maas[2]
William R. DeTar[3]

Introduction

Few papers have addressed the issue of detection or identification of field-level features in agricultural field crops with hyperspectral remote sensing (Green et al., 1998; Gat et al., 1999). Multispectral images have been used to identify certain field stresses and anomalies such as diseases, weeds, and mites (Brown et al., 1994; Peñuelas et al., 1995; Summy, et al., 1997) but the limited spectral coverage may not allow unique identification, only that an anomaly is present. The large amount of information available for analysis in hyperspectral imagery permits the application of advanced image analysis techniques designed to extract unique data features from high dimensional data sets and reduce complexity to make the data more interpretable. Spectral Mixture Analysis (SMA) assumes that a small number of spectra representing the scene components of interest (endmembers) can describe most of the spectral variation in a scene and be used to "unmix" the pixels and determine the relative fractional abundance of each component on a per-pixel basis. This approach could allow discrimination of one plant stress from another through identification of unique spectral features or differences in the shapes of the spectral curves. The abundance maps produced could indicate both the spatial extent and severity of stresses. This would permit a farm manager or scout to locate precisely the identified stress in a field, providing for guided field scouting and precision application of appropriate control measures such as pesticides or biological control agents. This procedure has been well documented in geological and ecological studies (Adams et al., 1995; Adams and Smith, 1986; Elmore et al., 2000; Mustard, 1993; Okin et al., 2001; Roberts et al., 1993; Roberts et al., 1998; Smith et al., 1990) but has had little to no application in precision agriculture.

The strawberry spider mite, *Tetranychus turkestani* causes severe damage to cotton in the San Joaquin Valley in California. These mites feed on plants causing leaf puckering and reddish discoloration in early stages of infestation and leaf drop later (Anonymous, 1996). Because of the leaf color change, and perhaps physiological changes not visible to the naked eye it was hypothesized that the spectral signature of mite-damaged leaves might provide a method to detect the pest. The objective of this paper was to develop ground-based reference spectral signatures of various scene components (endmembers) in field-grown cotton in order to unmix AVIRIS imagery using spectral mixture analysis and determine if the fraction maps could accurately discriminate between a field of healthy cotton and an adjacent field of mite-damaged cotton. Additionally, it was expected that the SMA procedure would provide endmember abundance fraction maps delivering spatially explicit maps of mite damage severity.

Materials and Methods

An experiment was established on two, 2.8 ha research fields at the USDA-ARS research station in Shafter, CA (35.5° N, 119.3° E., 120 meters above sea level). Each field was planted to cotton (*Gossypium hirsutum* L. variety "Maxxa") on May 4, 1999. Both were managed according to standard cultural practices for cotton in the area except that one (field 41) was sprayed once with a wide spectrum pesticide about eight weeks after planting, virtually eliminating mites as well as beneficial arthropods which normally keep mite populations in check. The other (field 42) was treated with appropriate pesticides several times during the growing season to control spider mite infestations. For reference, Figure 1 shows near-infrared images of fields 41 and 42 acquired from a high resolution multispectral system (Fitzgerald et al., 1999b) and one band from AVIRIS. Weekly mite counts were performed to monitor their temporal and spatial distribution within each of the fields (Anonymous, 1996). Visual

[1] USDA-ARS, U.S. Water Conservation Laboratory, Phoenix, Arizona gfitzgerald@uswcl.ars.ag.gov
[2] Dept. of Plant & Soil Science, Texas Tech University, Lubbock, Texas
[3] USDA-ARS, Western Integrated Cropping Systems Research Unit, Shafter, California

records were kept noting areas of obvious mite damage throughout the season. Both fields were irrigated with sub-surface drip irrigation leaving the soil surface dry all season.

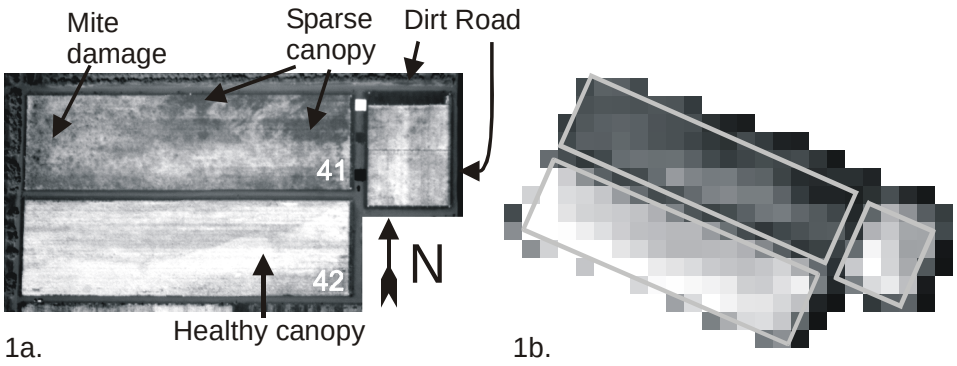

Figure 1a. High resolution (0.65 m) near-infrared image (850 nm) of cotton research fields 41 and 42 acquired on 25 Aug 1999. In field 41, mites were allowed to damage the cotton while in field 42 mites were controlled. Fields 41 and 42 each had dimensions of 100m X 300m. **Figure 1b**. AVIRIS image (band 41, 845 nm, 18 m pixel resolution) of the same fields acquired 28 Aug 1999.

A digital camera system consisting of visible and near-infrared "Varispec" liquid crystal tunable filters (LCTF) from Cambridge Research Instrumentation, Inc., Woburn, MA and a digital camera from PixelVision (Pluto model, 14-bit, cooled, 512 X 512 pixels) were mounted on a high clearance vehicle capable of entering cotton fields with the operator aboard a platform mounted on top. The liquid crystal filters are tuned electronically to allow narrow band wavelengths of light to pass through to the digital camera. The camera shutter and filter are synchronized so that an image is acquired when the filter switches to a new waveband. This system recorded images in 10 nm increments from 400 to 1050 nm. At a height of three meters above the soil, pixel resolution was about one mm. Images were calibrated to reflectance using a 99% "Spectralon" calibration panel which was placed in the field of view before and after image acquisition.

Imagery from AVIRIS was acquired for the research fields on four separate dates in 1999. Flight dates, local times, and solar zenith angle are shown in Table 1. The hyperspectral data cube from AVIRIS was composed of 224 images acquired contiguously from 400-2500 nm in approximately 10 nm bands. The AVIRIS data sets were atmospherically corrected and converted to reflectance using ATREM and EFFORT algorithms. Ground pixel resolution was 18 m.

Table 1. AVIRIS overflight dates, local times (PDT), and solar zenith angles.

Overflight Date	Local Time (PDT)	Solar Zenith
13 Jun 1999	11:29 am	22.7°
28 Aug 1999	12.09 pm	27.9°
1 Sep 1999	10:07 am	49.3°
24 Sep 1999	11:43 am	38.9°

Images acquired from the LCTF system were used to build a spectral library containing representative spectra (endmembers) that included sunlit healthy leaves (H), sunlit mite-damaged leaves (M), sunlit tilled soil (S), shaded tilled soil (Sh), and sunlit dead leaf (D). Pixels from each waveband representing the particular endmember (Fig. 2) were selected to build the spectral library (Fig. 3).

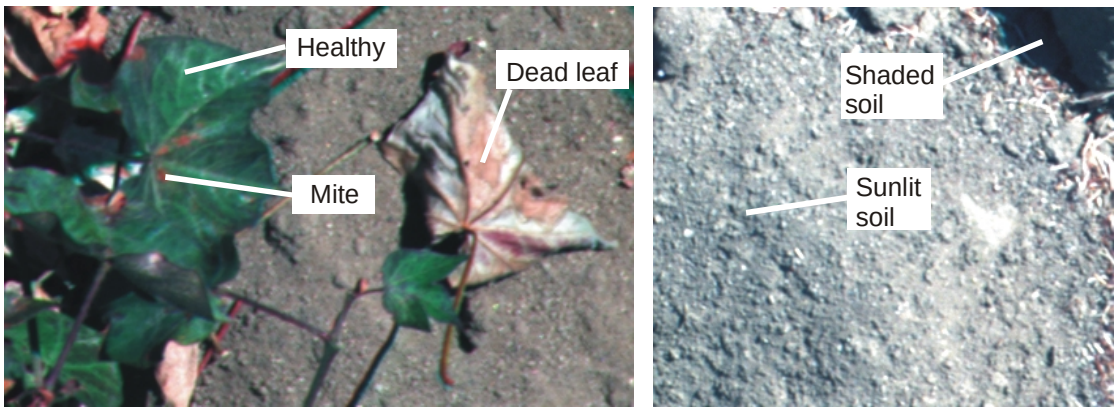

1a. 1b.

Figure 2. Liquid crystal tunable filter images showing scene components (endmembers). Each image represents about 0.15 m^2 (1.5 ft^2).

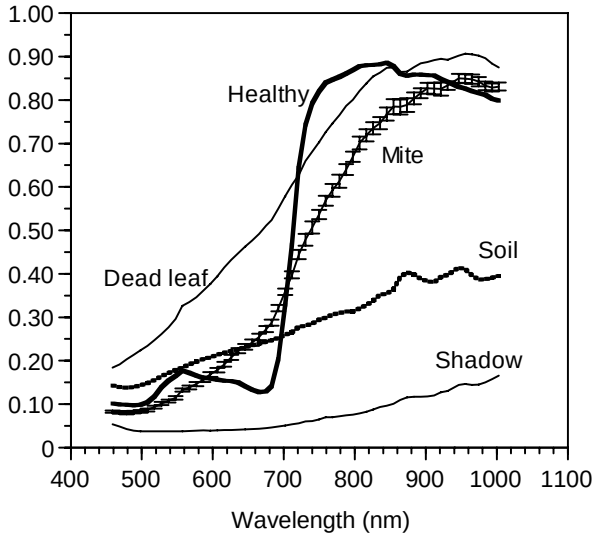

Figure 3. Spectral library endmembers derived from selected regions in the liquid crystal tunable filter imagery (see Figure 2). The error bars on the M endmember line represent ±1 standard error. Standard errors for the other curves were too small to show clearly.

The AVIRIS image cubes were masked to include only the fields of interest and then spectrally resampled to match the wavelengths of the LCTF spectral library. This resulted in 57 wavebands in 9.5 nm increments from 459 to 1002 nm. Spectral mixture analysis was then performed on the four AVIRIS images using the built-in linear spectral unmixing (LSU) routine in the ENVI software package (Better Solutions Consulting, Inc., Lafayette, CO). Analysis parameters were set to constrained unmixing with a weight of 10 which constrained the endmember fractions within each pixel to sum to unity. If the proper endmembers have been chosen for each pixel then the abundance fractions should be positive, the sum of all the abundance fractions (excluding the RMSE image) should equal unity, and the pixels should have a low RMSE (Smith et al., 1990; Roberts et al., 1998).

It was noticed in the fraction images that negative values occurred whenever a pixel contained an endmember that was not present at the time of image acquisition, e.g., pixels chosen over areas of known dense

canopy showed negative soil fractions or pixels from healthy vegetation (field 42) had negative M endmember fractions). Thus, a procedure was developed to assign variable numbers of endmember to the pixels. The criteria for assigning valid endmembers to each pixel was, 1) endmember sign (positive values retained, negative values assigned zero values), and 2) RMSE (whenever models of equal value occurred, the one with the lowest RMSE was selected). The number of potential endmembers was limited because the fields were not as heterogeneous as, say a regional image containing roads, lakes, urban features, etc. as discussed in Roberts et al. (1998). Thus, based on knowledge of the field and the fact that the objective of the study was to identify mite areas only, the five endmembers in Figure 3 were chosen as those representing the bulk of the variance in the fields. The iterative process to choose variable number of endmembers per pixel began with the five endmembers and flagged pixels with negative endmembers. The flagged pixels were re-analyzed with four endmembers, followed by three and two endmember models, consecutively. At each stage, if a set of endmembers was equally valid (e.g., two, three-endmember models contained positive values) then the one with the lowest RMSE was selected. This continued until all pixels were assigned endmembers.

Results

The combination of endmembers that consistently had the lowest RMSE, summed to unity, and correctly located known areas of mite damage, healthy plants, and soil was the combination that included the S, M, H, and Sh endmembers, except for the 13 Jun image that did not include the Mite endmember because mites were not present. Whenever Sh was excluded from the unmixing analysis, the sum of endmember abundances ranged from 0.60 to 0.92. When Sh was included, all pixel abundances summed from 0.99 to 1.00. A spectrum representing dead leaves was initially included in the unmixing procedure to account for non-photosynthesizing vegetation (NPV) but fraction values were always negative so they were excluded from further analysis.

Pixels forming Regions of Interest (ROI) were visually selected for field 41, field 42, and the dirt road around the fields. These represented the mite-damaged canopy, healthy canopy, and soil/dirt road areas, respectively. Table 2 shows the mean values of these regions and Figure 4 shows the abundance image maps indicating the spatial distribution and intensity of these endmembers (bright pixels indicate high abundance fraction values and black pixels equal zero).

Table 2. Fractional abundance means by endmembers for Regions of Interest selected within fields 41, 42, and the dirt roads surrounding the cotton fields. Zero values indicate absence of endmembers.

Field 41	13 Jun 99	28 Aug 99	1 Sep 99	24 Sep 99
Soil	0.650	0.012	0	0.027
Mite	0	0.092	0.010	0.044
Healthy	0.043	0.344	0.240	0.280
Shade	0.307	0.552	0.750	0.649
RMSE	0.018	0.021	0.016	0.015
Field 42				
Soil	0.650	0	0	0
Mite	0	0	0	0.020
Healthy	0.046	0.630	0.400	0.401
Shade	0.304	0.370	0.600	0.579
RMSE	0.019	0.053	0.042	0.027
Road				
Soil	0.882	0.715	0.464	0.576
Mite	0	0	0	0
Healthy	0	0.073	0.049	0.070
Shade	0.117	0.212	0.486	0.354
RMSE	0.027	0.018	0.019	0.015

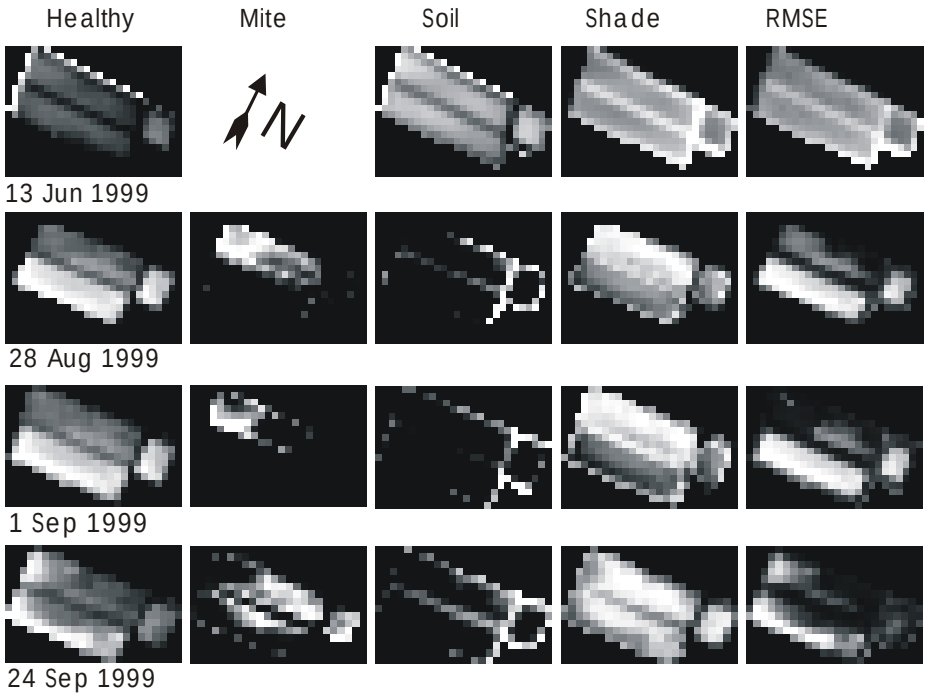

Figure 4. Fractional abundance image maps produced from spectral unmixing of the four AVIRIS image cubes. Highest to lowest values are represented by brightest to darkest pixels. Black pixels have zero value. All values were zero for the M endmember abundance map on 13 Jun 1999.

On 13 Jun 1999, the mean values from the two fields for the four endmembers and RMSE were essentially the same (Table 2). This was expected since mite damage had not yet occurred and all other factors were equal (irrigation, planting date, cultural practices, etc.). By 28 Aug 1999, mites had been present for seven weeks and the unmixing procedure correctly showed that field 41 had mite-damaged cotton plants whereas field 42 did not. Since the 1 Sep 1999 overflight occurred only four days later, little difference should be expected between the two in terms of relative endmember fractions. The differences in endmember fractions noted in Table 2 between the two dates can be attributed to the amount of Sh fraction. The solar zenith angle was much greater for 1 Sep than 28 Aug (Table 1) resulting in a greater Sh component and consequently lower fraction values for the other endmembers. The relative differences however were maintained (H > M > S). Pixels with greater M fraction values were located in the same areas in field 41 on both dates (Fig. 4) showing a consistent pattern.

By 24 Sep 1999, a few weeks before harvest, senescence became a dominant feature. Some pixels in Figure 4 are brighter for the M endmember and darker for the H endmember in field 42. Also, the location of bright pixels for the M images in field 41 (Fig. 4) changed from the previous two dates. When cotton senesces, it tends to form red spots on its leaves. The spectral signature from the reddish senescent vegetation undoubtedly resembled that of the M endmember (Fig. 3).

The S fraction was always greatest for the Road region and non-existent in field 42 once full canopy was established (Table 2). The dirt roads around the fields are clearly identified in the S fractions in Figure 4. Some vegetation was present in the pixels selected for the Road ROI as evidenced by small positive H endmember values in Table 2. This is reasonable since the 18m pixels would have encompassed edges of the fields as well as road.

The Sh endmember pixels were brightest where there was more canopy variability along the edges of the fields and in the mite infested and sparse canopy regions where there was a mix of canopy and soil (Fig. 4). The mean Sh fraction values were always greatest in field 41 and lowest in the Road ROI within a given date (Table 2). This seems to indicate there was more shade in more heterogeneous parts of the scene, a reasonable outcome.

The highest RMSE values occurred for healthy vegetation, for example in field 42 (Table 2, Fig. 4) probably due to calibration errors between the LCTF and AVIRIS imagery. The H endmember spectrum differed somewhat from the healthy canopy spectrum derived from the AVIRIS imagery (not shown). However, shapes of the curves were fundamentally similar showing the characteristic red edge and green peaks. It is likely the greater RMSE for the H endmember was due to imperfect curve fitting by SMA. Despite this, the routine is obviously robust enough to match the endmember and AVIRIS spectra, and overall results show good correlations to known ground conditions.

Discussion

Mite detection early in the season is critical if the farm manager is to use imagery as a decision aid for control. In this respect, these AVIRIS images are not useful since the acquisition times did not correspond to early mite infestations and the large pixel size would not allow early identification of a few mite-infested plants occupying a minute percentage of a pixel, even using SMA techniques. Additionally, under normal farming practices, mite damage would never be allowed to progress to the degree of damage present in field 41. However, these conditions were advantageous for mite detection in this study because of the contrast between severe and light or non-existent mite damage in the two fields and the spatially extensive damage within field 41.

There are several measures of success for the unmixing procedure in this analysis. One, the plant and soil conditions in field 41 and 42 were essentially the same on 13 Jun so it is encouraging to find the mean fraction values for these fields are so similar. Two, there were no false positives for selection of the M endmember in field 42. All M endmembers were selected in field 41. Three, the S fraction consistently was greatest over the dirt road and showed low values in field 41 but was not present in field 42 once full canopy was established. Four, the relative brightness and locations of abundance fractions from 28 Aug and 1 Sep, which were acquired only four days apart, are similar (Fig. 4). However, because the solar zenith angles are different, the abundance fractions are not the same (Table 2). It appears that it can be difficult to compare the abundance fractions across dates. There may be a temporal or non-linear component tied to the shade endmember since this changed with zenith angle and the Sh fraction differed on each date. Perhaps other shade endmembers should have been included in the analysis, such as shaded healthy leaves and shaded mite-damaged leaves.

The LSU procedure in the ENVI software outputs images with the same number of endmembers for every pixel. This is not realistic since there is spatial variability across images not just in terms of quantity (endmember abundance) but also in quality (which endmembers are present). Removing unrealistic (negative) endmembers resulted in pixels with varying numbers of endmembers (2-4) and is similar conceptually to the multiple endmember selection method presented by Roberts et al. (1998). The result shows abundance images that match known ground conditions. This procedure therefore incorporated both spectral and spatial variability. The comparison across four dates allowed a measure of temporal change to be incorporated into the analysis which is critical for agriculture. The resulting images showed both consistent features and explainable changes in the crop (Fig. 4).

In the near future, high spatial resolution hyperspectral imagery will be available that can pinpoint with greater accuracy the locations of stressed plants. Frequent image acquisition would allow temporal changes to be monitored, and early signs of problems could be detected. The utility of hyperspectral remote sensing for precision agriculture comes, in part, from the potential to identify stressed areas in fields early enough for the farm manager to make timely decisions. However, it remains to be seen whether early detection can be accomplished and is, therefore, a fertile area for research.

Disclaimer and Acknowledgments

Mention of specific suppliers of hardware and software in this manuscript is for informative purposes only and does not imply endorsement by the United States Department of Agriculture. Thanks to Nahum Gat at Opto-Knowledge Systems, Inc. for calibrating AVIRIS data, supplying the liquid crystal tunable filter camera system, and technical support.

This research was supported, in part, through the NASA SSC Hyperspectral EOCAP project and a grant from Cotton, Incorporated. AVIRIS flights were provided by the Jet Propulsion Laboratory, Pasadena, California.

Literature Cited

Adams, J.B., and Smith, M.O. (1986), Spectral mixture modeling: A new analysis of rock and soil types at the Viking Lander 1 Site, *J. Geophys. Res.* 91:8098-8112.

Adams, J.B., Sabol, D.E., Kapos, V., Filho, R.A., Roberts, D.A., Smith, M.O., and Gillespie, A.R. (1995), Classification of multispectral images based on fractions of endmembers: Application to land-cover change in the Brazilian Amazon, *Remote. Sens. Environ*. 52:137-154.

Anonymous (1996), Integrated pest management for cotton in the western region of the United States, 2nd edition. University of California, Division of Agriculture and Natural Resources, 164 pgs.

Brown, R.B., Steckler, J.-P.G.A., Anderson, G.W. (1994), Remote sensing for identification of weeds in no-till corn, *Transaction of ASAE* 37:297-302.

Elmore, A.J., Mustard, J.F., Manning, S.J., and Lobell, D.B. (2000), Quantifying vegetation change in semiarid environments: Precision and accuracy of spectral mixture analysis and the normalized difference vegetation index, *Remote Sens. Environ.* 73:87-102.

Fitzgerald, G.J., Maas, S.J. and Detar, W.R. (1999b), Detection of spider mites in cotton using multispectral remote sensing, In *Proc. 17th Biennial Workshop on Color Photography and Ideography in Resource Assessment*, Reno, Nevada, 5-7 May, pp. 77-82.

Gat, N., Erives, H., Maas, S.J., and Fitzgerald, G.J. (1999), Application of low altitude AVIRIS imagery of agricultural fields I the San Joaquin Valley, CA to precision farming, In *Summaries of the 8th JPL Airborne Earth Science Workshop*, (R.O. Green, Ed.), Pasadena, California, 9-11 Feb., pp. 145-150.

Green, R.O., Pavri, B., Roberts, D., and Ustin, S. (1998), Mapping agricultural crops with AVIRIS spectra in Washington State, In *Summaries of the 7th JPL Airborne Earth Science Workshop*, (R.O. Green, Ed.), Pasadena, California, Jan. 12-16, pp. 213-220.

Mustard, J.F. (1993), Relationships of soil, grass, and bedrock over the Kaweah Serpentine Melange through spectral mixture analysis of AVIRIS data, *Remote Sens. Environ.* 44:293-308.

Okin, G.S., Roberts, D.A., Murray, B., and Okin, W.J. (2001), Practical limits on hyperspectral vegetation discrimination in arid and semiarid environments, *Remote Sens. Environ.* 77:212-225.

Peñuelas, J., Filella, I., Lloret, P., Munoz, F., and Vilajeliu, M. (1995), Reflectance assessment of mite effects on apple trees, *Int. J. Remote Sens.* 16(14):2727-2733.

Roberts, D.A., Smith, M.O., and Adams, J.B. (1993), Green vegetation, non-photosynthetic vegetation, and soils in AVIRIS data, *Remote Sens. Environ.* 44:255-269.

Roberts, D.A., Gardner, M., Church, R., Ustin, S., Scheer, G., and Green, R.O. (1998), Mapping Chaparral in the Santa Monica mountains using multiple endmember spectral mixture models, *Remote Sens. Environ.* 65:267-279.

Smith, M.O., Ustin, S.L., Adams, J.B., and Gillespie, A.R. (1990), Vegetation in deserts: I. A regional measure of abundance from multispectral images, *Remote Sens. Environ.* 31:1-26.

Summy, K.R., Everitt, J.H., Escobar, D.E., Alaniz, M.A., and Davis, M.R. (1997), Use of airborne digital video imagery to monitor damage caused by two honeydew-excreting insects on cotton, In Proc. *16th Biennial Workshop on Color Photography and Videography in Resource Assessment*, 29 Apr.-1 May, pp.238-244.